INSTITUTE OF PLASMA PHYSICS

NAGOYA UNIVERSITY

Collision experiment on highly ionized ions using vacuum spark source

S. Takagi*, S. Ohtani, K. Kadota

and J. Fujita

(Received - Mar. 9, 1982)

IPPJ-564 Mar. 1982

RESEARCH REPORT

NAGOYA, JAPAN

Collision experiment on highly ionized ions using vacuum spark source

S. Takagi*, S. Ohtani, K. Kadota
and J. Fujita

(Received - Mar. 9, 1982)
IPPJ-564 Mar. 1982

Further communication about this report is to be sent to the Research Information Center, Institute of Plasma Physics, Nagoya University, Nagoya 464, Japan

---

* Permanent address: Department of Electric Engineering,
Doshisha University,
Kyoto 602, Japan.

Abstract

Cross sections for one-electron capture by Fe^{6+} in H_2 are measured below 10 keV by using a vacuum spark ion source. It is found that the cross sections show little dependence on the collision energy and this value is about $6 \times 10^{-15} cm^2$. This ion source, which has no electrode for ion extraction, can produce ions from several hundreds eV to several tens of keV and the maximum charge state of 16 in Fe at 125J discharge energy. With ion selection system of 2.7m time-of-flight and an electrostatic analyzer of 1% resolving power, 10^2-10^3 ions/pulse are obtained. Because of poor reproducibility of ion beam, charge-transferred ions and unreacted ions are measured simultaneously with a microchannel plate which has two anodes behind. By utilizing the feature of pulsed ion beam and this ion selection system, it is possible to obtain cross sections for various charge states of ions simultaneously.

1. Introduction

Recently electron-capture for multicharged ion has drawn attention in both atomic physics and applications [1] of electron-capture to fusion research, astrophysics and X-ray laser. The reaction leads generally to not only change of ionic state of projectiles but also energy loss in collision system, because electron-capture is accompanied with photon emission, which is caused by capture of an active electron into an excited state [2,3,4,5,6,7,8]. Especially electron-capture processes on multicharged ions play an important role in various field. For example, a study of electron-capture processes of the type

$$X^{q+} + H \rightarrow X^{(q-1)+} + H^{+} \qquad (1)$$

is important in investigating energy and particle losses from high-temperature plasmas [9]. The cross sections in several tens of keV are necessary for additional heating of plasma by the injection of fast neutral beam [10]. The data in the lower energy are necessary for a study of interaction of impurity ions and thermalized atoms. Also a study of edge plasmas necessitates low energy data. As light impurity ions X^{q+} in the charge transfer reaction (1), C, N and O are of interest. As heavy impurity ions, there are metallic species sputtered from the wall. With the increase of plasma temperature, the problem of energy loss becomes more important for heavy metallic ions than ions of light elements [11].

The cross sections for highly ionized ions are not

sufficiently measured in low energy, since it is difficult to generate these ions. With the improvement of some kinds of sources, namely, EBIS type ion source [12], RF ion source [13] and secondary ion recoil source [14], the cross sections on light elements have been obtained in low energy. On heavy metallic elements the cross sections are scarecely obtained. McCullough et al. measured cross sections for one-electron capture by doubly charged ions of Ba, Ti, Mg, Cd and Zn in H and H_2 in the energy range 0.8 - 40 keV with a sputtered ion source. Crandall et al. measured cross sections for one-electron capture by $Fe^{5,6+}$ in H and H_2 in the energy range of several tens of keV, using a PIG type ion source.

We paid attention to a vacuum spark as low energy multicharged ion source. An ion source of this type was first used by Zwally [17] in order to study one-electron capture for C^{4+} in He, Ne and Ar. This type of ion source can easily generate heavy metallic multicharged ions at low energy, but has many defects of a very short duration of an ion pulse, a low repetition rate, generation of high frequency noise and poor reproducibility [18]. After overcoming these problem, we used a vacuum spark as a heavy metallic ion source in low energy. In this paper, some characteristics of the vacuum spark ion source and the experimental apparatus for collision experiments are described. The cross sections for one-electron capture by Fe^{6+} in H_2 have been measured below 10 keV, using this experimental setup.

2. Vacuum spark type ion source

A schematic diagram of a vacuum spark type ion source is shown in fig.1. A cathode of 5 mm in diameter separated by 5mm from an anode tip of 5 mm diameter is used, with a metallic cylinder serving as a current return from the cathode to 10.4 μF capacitor (maximum operation voltage 20 kV). The inductance experimentally obtained is 150 nH in the whole discharge circuit. The discharge is triggered by the use of a pulsed YAG laser beam which is focused onto the anode through an axial hole in the cathode. Evaporation of the anode material due to the irradiation of the laser beam plays a role of a fast-acting gas injection [19]. The maximum discharge current is about 100 kA in 2.5 μsec at 1 kJ discharge. The discharge chamber is evacuated to a pressure of 1×10^{-6} torr. This device produces a hot plasma concentrated at a point (or frequently several points) near the anode tip, as confirmed by pinhole X-ray photographs [19,20,21,22]. The electron temperature and density of the hot plasma are estimated to be $\sim 10^{21}$ cm^{-3} and $\sim$ 10 keV, respectively [19,20,23,24]. The life time is below several tens of nanosecond [19]. The highly ionized ions of the anode material are included in the hot plasma, as evidenced from the X-ray spectroscopy [19,20,22,24].

A part of the hot plasma expanding perpendicularly to the discharge direction enters a drift space of field free region. The charge state- and velocity- selection for the highly ionized ions are performed by using conbined time-of-flight (TOF) and electrostatic analysis. Figure 2 shows the analysis system, which

has a gas cell and an electrostatic deflector in order to be applied to atomic collision experiments. The electrostatic analyzer used is of 127° deflection type. Symmetric voltages are applied to the deflecting plates of the analyzer. The plasma density is so low at the front of the electrostatic analyzer that space charge and Debye screening effects are negligible, and therefore electrostatic control can be performed for the q/E analysis. The path length of TOF is 2.7 m. The analyzer is followed by a microchannel plate (MCP) as an ion detector. In this experiment, several hundreds ions are incident upon a detector for the interval less than 1 μsec. Since the average time interval of the ion arrival is $10^{-9} \sim 10^{-10}$ sec, it is difficult to use a counting method. The total current from the MCP is observed with an oscilloscope through a coupling condenser. The signal is integrated with a resister of 10 kΩ and a stray capacitance of 120 pF. The reason why a MCP was selected as a detector and the way of its operation are described in the next section.

A typical TOF spectrum of C^{q+} ions at E/q = 1.25 keV is shown in fig.3, where graphite is used as anode material. In this figure, an impurity peak of hydrogen is observed at M/q = 1, which is considered to be absorbed into the graphite anode. The number of ions per pulse is estimated to be from several hundreds to one thousand. By observing TOF spectrum for various analyzer voltage, velocity distributions in each ionic state are obtained. Since the bandwidth of the energy analyzer depends on the selected energy, it is necessary to compare the ion flux in the same energy bandwidth. The ion flux observed is transformed

to the flux in the same energy bandwidth by dividing the intensity of the ion flux by the energy on the bandwidth. Furthermore, it is necessary to consider the dependence of the detection efficiency on charge states and velocities of incident ions. A detector of a channel electron multiplier type is operated at so high gain, that if an incident ion ejects at least one secondary electron, the space charge density at the output of the channel is determined by the space charge limit [25]. For the incident energy over 1 keV, the detection efficiency is expected to be equal for the kinds of incident ions, since the yield of secondary electron emission at the ion input is more than unity. But for the incident energy below 1 keV, the relative intensity of each velocity distribution contains significant error, since the yield becomes less than unity [26].

Fig.4 shows the velocity distributions of C^{q+} ions at the discharge energy of 45 J. It is shown that the emerging ions have a wide range of velocities. In this velocity range, the vacuum spark can be used as a multicharged ion source without any additional acceleration or deceleration system. When iron is used as anode material, the velocity distributions of Fe^{q+} ions are shown in fig.5. Each figure represents the distributions at the discharge energies of 24 J, 45 J and 125 J. In order to remove complications in these figures, distributions for not all of the charge states are drawn. The maximum charge state detected is 16 at 125 J discharge energy. As the operation voltage increases, ions of higher charge states and velocity appear. With the increase of ionic states, energy spread of ions become narrow. An electrode for ion extraction must be set in the case of need.

3. Application to an atomic collision experiment

The experimental apparatus is shown in fig.2. A gas cell and a deflector are added to the ion analysis system. Ions from the source are selected according to E/q and M/q with electrostatic analyzer and TOF, and enter the target gas cell. After passing through the gas cell, the ions are separated according to their charge states with an electrostatic field. The charge-transferred ions and the ions of an initial charge state are detected simultaneously with the MCP which has two anodes behind. In order to prevent the interference of two kinds of electrons generated by these two kinds of ions, a dead zone of 2 mm width is provided at the boundary of these areas by setting a metallic foil of 2 mm width in front of the MCP. The input of the MCP is grounded, so that charge-transferred ions enter the MCP at the same velocity as primary ions. The MCP used in this experiment is type F 1158-11 (Hamamatsu TV). The diameter of an individual pore of the MCP is 12 μm and the ratio of the length to the diameter is 45. The 127° electrostatic analyzer and the deflector are calibrated with a Li^+ ion source of thermionic emission type using β-eucryptite.

The reason why we used a MCP is as follows. As for the detector, it is necessary to investigate the linearity between an output and the number of an incident ions and to investigate detection efficiencies on various charge states. In a MCP, after a channel fires by incidence of a particle or a photon, the charge is replenished in the channel wall. Since the recovery time is about 100 msec in the MCP [25] and the pulse width of ion

beam is less than 1 μsec, a channel can detect only an ion. Therefore the linearity between the output current and the number of ions can be determined from the relation between the number of channels and the number of incident ions. If the number of channels is much more than the number of incident ions, the linearity is ensured. The cross section of a beam at the position of the MCP is inferred about 4.2 mm^2. In this area there are about 20000 channels. Since the number of ions is about 1000, it is considered that the linearity is good. On the detection efficiency, as mentioned above, it is considered that the detection efficiency of a MCP is independent of a charge state of an incident ion above 1 keV. Actually, when we investigated the pulse height distributions of a MCP on various charge state, the results had a tendency that an ion of higher charge state had a higher pulse height. This result will be reported elsewhere. This effect is treated as one of uncertainties. In comparison with a MCP, a channel electron multiplier (CEM) has a cone to detect a broad beam. Some kinds of CEMs show a different detection efficiency when an impact position of a beam is different. Since a MCP deos not have a cone, such phenomenon does not appear [27]. A MCP is suitable for multichannel detection because it is not necessary to use many detectors.

The size of slits which locate in the region from the entrance of the 127° electrostatic analyzer to the entrance of the deflector are as follows: the entrance of the electrostatic analyzer (width: 0.5 mm, height: 15 mm), the exit of the analyzer (width: 1.8 mm, height: 5 mm), the entrance of the gas cell (width: 1 mm, height: 2.8 mm), the exit of the gas cell (diameter: 2.8 mm^{ϕ}),

the entrance of the deflector (width: 9mm, height: 9.5 mm).

The situation that ions are deflected by the deflector is shown in fig.6, which shows an example of carbon ion. A multiple-electron capture is not considered in this experiment. By observing both charge-transferred ions and ions of an initial charge state with respective detectors, it is possible to measure simultaneously cross sections for all ion species selected with the 127° electrostatic analyzer. Actual signals are shown in Figures 7 and 8. Iron and H_2 gas are used as anode material and a target gas, respectively, and collision energy is 1.75q keV. Figs. 7 and 8 represent signals obtained at pressures of 3×10^{-6} torr (residual gas) and 4.4×10^{-5} torr (H_2 gas), respectively. In the both figures, (a) and (b) represent signals of the ions of an initial charge state and charge-transferred ions, respectively. In fig.6 C^{q+} ions appears as impurity ions because carbon was used before the use of the iron anode. The cross sections calculated from these figures contain large error, since two kinds of ion beams can not be separated. When the gas is not supplied to the gas cell, the beam width is about 1.5 mm at the position of the detector. When the gas is supplied, the charge-transferred beam are slightly spread and also a part of ions of initial charge state are spread by an elastic collision. Assuming that the beam spread is determined by the length (14 cm) and the exit slit width of the gas cell, the beam width is about 8 mm at the position of the detector. In order to measure the charge-transferred ion of various charge states in this measurement, the MCP of 20 mm in diameter is divided in the ratio 4:1. In this system the care must be taken in the relation between beam

width and the size of the detector. When cross sections for one-electron capture by Fe^{6+} in H_2 are measured, the MCP is divided into two halves. In each part, the ions of an initial charge state (Fe^{6+}) and the charge-transferred ions (Fe^{5+}) are detected, respectively.

Under a single collision condition, a cross section is obtained from the following formula

$$\sigma_{i,i-1} = \frac{1}{nl} \ln \frac{\alpha_{i-1} I_{i-1} + \alpha_i I_i}{\alpha_i I_i} \qquad (2)$$

where n is the density of the target gas and l is the effective length of the gas cell. I_{i-1} and I_i are the intensities of ions of ionic charges i-1($A^{(i-1)+}$) and i(A^{i+}) after passing through the gas cell. α_{i-1} and α_i are the detection efficiencies for $A^{(i-1)+}$ and A^{i+} ions. In this experiment, it is assumed that the detection efficiency of the MCP is identical for all the ions with different charge states. If a multiple-electron transfer is neglected in this experiment, $I_i + I_{i-1}$ represents the intensity of the primary ions.

The cross sections for one-electron capture by Fe^{6+} in H_2 are measured in the energy range from 3 keV to 10.5 keV. Figure.9 shows $\ln[(I_6+I_5)/I_6]$ as a function of the target thickness. In this figure the value of $\ln[(I_6+I_5)/I_6]$ is the average of 8 shots and the error bar represents the standard deviation. The gradient is calculated using a method of least squares. The target density n is determined by the use of an ionization gauge attached to the cell, which is calibrated by a capacitance manometer (MKS Baratron) for H_2 gas. The collision length is assumed to be the distance between the entrance and exit slits.

The cross section for one-electron capture by Fe^{6+} in H_2 are shown in fig.10 as a function of a collision energy. In this energy range, the data show little dependence on the collision energy. (●) represents the present results and (○) the results of Crandall et al. [16].

Most of uncertainties come from the measurements of the primary and product ions and the effect of angular divergence of the beam detected. The maximum uncertainty caused by reading the level of the signal from the oscilloscope trace is $\pm$20 %. The uncertainty associated with determination of the slope of the intensity ratio curve is less than $\pm$10 %. The uncertainty of $\pm$ 15 % is estimated due to the effect which comes from failing to detect the primary and product ions due to the beam divergence or scattering associated with the electron capture. Further uncertainties arise from pressure calibration ($\pm$5 %), beam purity ($\pm$5 %) and the target cell end correction ($\pm$2 %). The total uncertainty for the absolute value of the cross section is estimated to be less than $\pm$30 % in quadrature sum. Furthermore, in addition to this uncertainty, there may be systematic error which arises from the dependence of detection efficiency of the MCP on the ionic charge state. According to the preliminary measurement, the maximum error which comes from this effect is estimated to be +15 %, -0 %.

4. Conclusion

The vacuum spark has been successfully used for collision experiments as a heavy metallic ion source, after solving some experimental problem associated with this source. Using this source, cross sections for one-electron capture by Fe^{6+} in H_2 have been measured below 10 keV. The results show little dependence on the collision energy and the value is about 6×10^{-15} cm^2.

5. Acknowledgments

The authors are grateful to Professor H. Tsuda, Doshisha University, for continuous encouragement through this work. Thanks are also due to Dr. J. Mizui and Mr. S. Morita for many helpful discussions. The authors wish to thank Mr. Y. Kawasumi for useful advice in designing the apparatus.

References

1) D.H. Crandall, Electronic and Atomic Collisions (ed. N. Oda and K. Takayanagi, North-Holland, 1980) p 387

2) M.W. Siegel, Y.H. Chen and J.W. Boring, Phys. Rev. Lett. 28 (1972) 465

3) A. Niehaus and M.W. Ruf, J. Phys. B 9 (1976) 1401

4) J.A. Guffey, L.D. Ellsworth and J.R. Macdonald, Phys. Rev. A15 (1977) 1863

5) H. Winter, E. Bloemen and F.J. de Heer, J. Phys. B 10 (1977) L599

6) V.V. Afrosimov, A.A. Basalaev, G.A. Leĭko and M.N. Panov, Zh. Eksp. Teor. Fiz. 74 (1978) 1605 [Sov. Phys. JETP 47 (1978) 837]

7) P.H. Woerlee, T.M. El. Sherbini, F. J. de Heer and F.W. Saris J. Phys. B 12 (1979) L235

8) R. Mann, F. Folkmann and H.F. Beyer, J. Phys. B 14 (1981) 1161

9) A. Lorenz, J. Phillips, J.J. Schmidt and J.R. Lemley, INDC (NDS)-72/LNA (1976)

10) D.R. Sweetman, Nucl. Fusion 13 (1973) 157

11) R.V. Jensen, D.E. Post, W.H. Grasberger, C.B. Tarter and W.A. Lokke, Nucl. Fusion 17 (1977) 1187

12) Y. Kaneko, T. Iwai, S. Ohtani, K. Okuno, N. Kobayashi, S. Tsurubuchi, M. Kimura and H. Tawara, J. Phys. B 14 (1981) 881

13) S. Bliman, N. Chan-Tung, S. Dousson, B. Jacquot and D. Van Houtte, Phys. Rev. A21 (1980) 1856

14) C.L. Cocke, R. DuBois, T.J. Gray, E. Justiniano and

C. Can, Phys. Rev. Lett. 46 (1981) 1671

15) R.W. McCllough, W.L. Nutt and H.B. Gilbody, J. Phys. B 12 (1979) 4159

16) D.H. Crandall, R.A. Phaneuf and F.W. Meyer, Phys. Rev. A22 (1980) 379

17) H.J. Zwally and D.W. Koopman, Phys. Rev. A2 (1970) 1851

18) H.J. Zwally, D.W. Koopman and T.D. Wilkerson, Rev. Sci. Instr. 40 (1969) 1492

19) T. N. Lee, Astrophys. J. 190 (1974) 467

20) L. Cohen, U. Feldman, M. Swartz and J.H. Underwood, J. Opt. Soc. Am. 58 (1968) 843

21) C.R. Negus and N.J. Peacock, J. Phys. D 12 (1979) 91

22) B.S. Fraenkel and J.L. Schwob, Phys. Lett. 40A (1972) 83

23) J.L. Schwob and B.S. Fraenkel, Phys. Lett. 40A (1972) 81

24) J.J. Turechek and H.J. Kunze, Z Physik A273 (1975) 111

25) J.L. Wiza, Nucl. Instr. and Meth. 162 (1979) 587

26) D.H. Crandall and J.A. Ray, Rev. Sci. Instr. 46 (1975) 562

27) J.A. Panitz and J.A. Foesch, Rev. Sci. Instr. 47 (1976) 44

Figure captions

Fig.1 A schematic diagram of the vacuum spark type ion source. Yhe discharge is triggered by the use of a pulsed YAG laser beam which is focused onto the anode through an axial hole in the cathode.

Fig.2 A schematic diagram of the experimental apparatus.

Fig.3 TOF spectrum in the use of a carbon anode. The energies of ions are 1.25 q keV.

Fig.4 The velocity distributions for C^{q+} ions at 45 J discharge energy. — -- —; C^{+}, — - — ; C^{2+}, — — — ; C^{3+}, —— ;C^{4+}, ----- ; C^{5+}.

Fig.5 The velocity distributions for Fe^{q+} ions at the discharge energies of 24 J, 45 J and 125 J. In order to remove complications, the distributions for not all of the charge states are drawn.

Fig.6 The conceptual drawing of separating the charge-transferred ions from the primary ions in the case of C^{q+} ions.

Fig.7 TOF spectrum in the use of an iron anode at 45 J discharge energy. The signals (a) and (b) represent the ions of the initial charge state and the charge-transferred ions. The ion energies are 1.75 q keV. A pressure in the gas cell is 3×10^{-6} torr (residual gas).

Fig.8 TOF spectrum in the use of an iron anode at 45 J discharge energy. The signals (a) and (b) represent the ions of the initial charge state and the charge-transferred ions. The ion energies are 1.75 q keV. A pressure in the gas cell is 4.4×10^{-5} torr (H_2 gas).

Fig.9 $\ln[(I_6+I_5)/I_6]$ as a function of the target thickness at collision energy of 4.5 keV. Error bars represent standard deviation.

Fig.10 The cross sections for one-electron capture by Fe^{6+} in H_2. ● ; Present results, ○ ; Crandall et al.

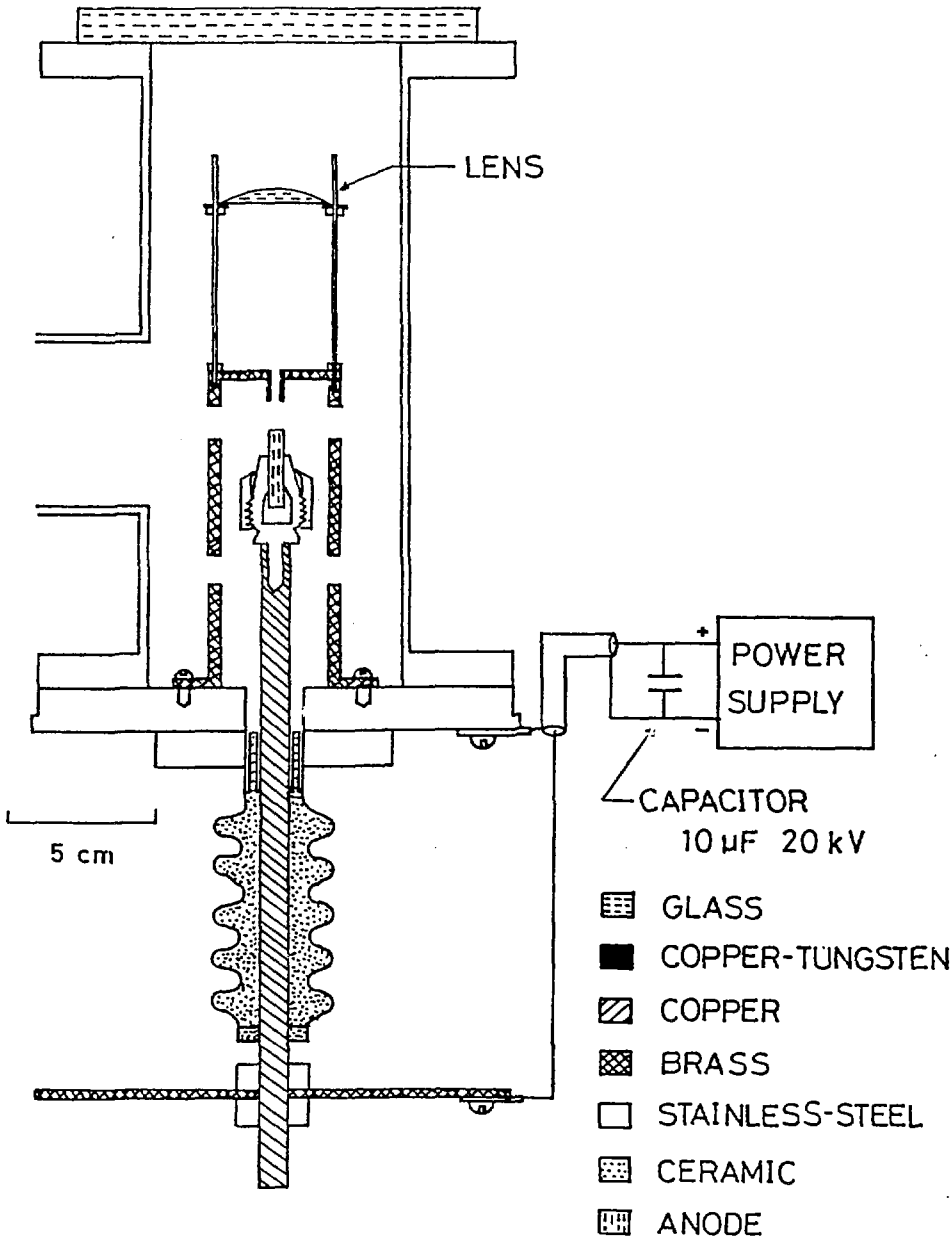
LENS
POWER
SUPPLY
+
−
CAPACITOR
10 μF 20 kV
5 cm
GLASS
COPPER-TUNGSTEN
COPPER
BRASS
STAINLESS-STEEL
CERAMIC
ANODE

Fig. 1

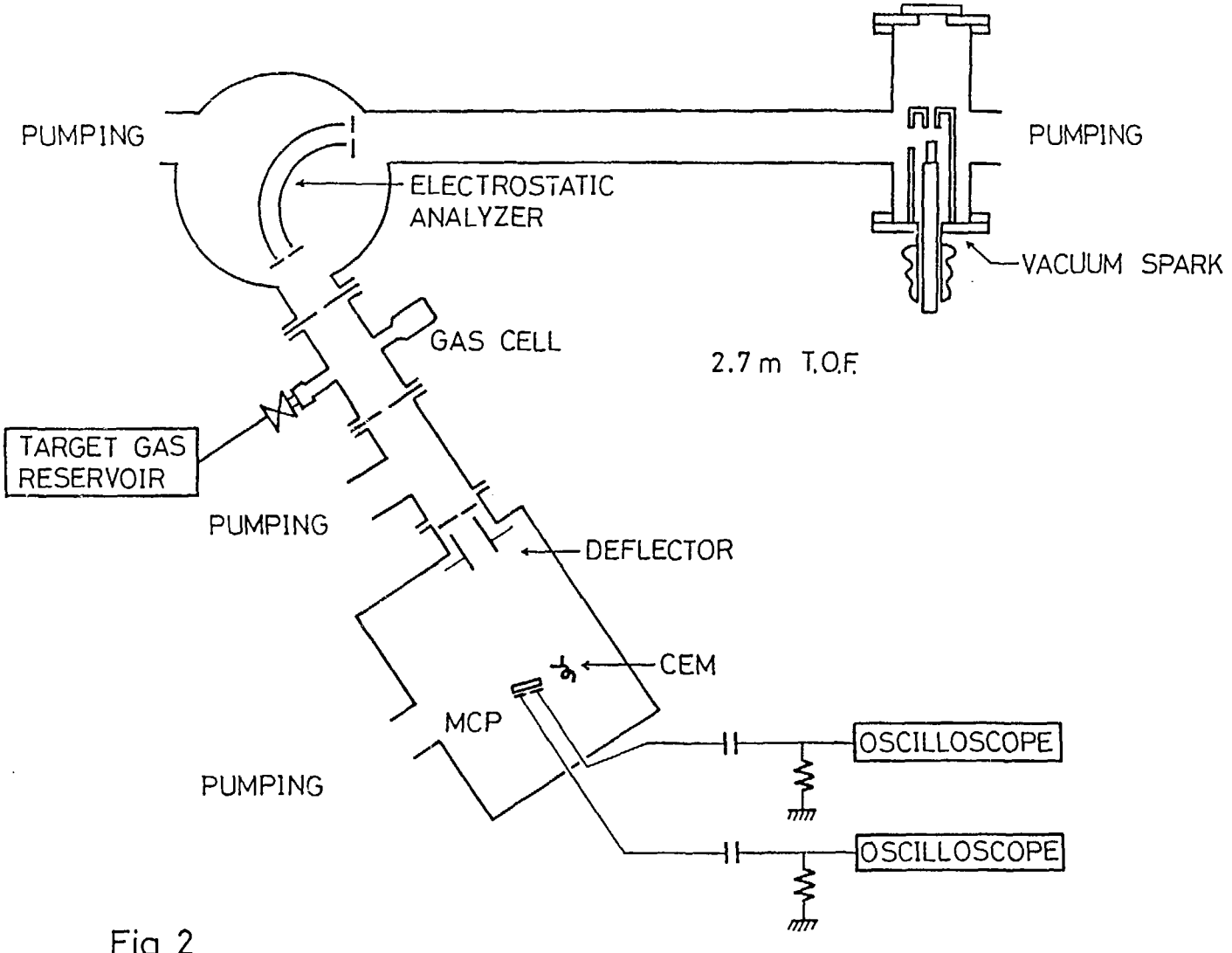
PUMPING
PUMPING
ELECTROSTATIC
ANALYZER
VACUUM SPARK
GAS CELL
2.7 m T.O.F.
TARGET GAS
RESERVOIR
PUMPING
DEFLECTOR
CEM
MCP
PUMPING
OSCILLOSCOPE
OSCILLOSCOPE

Fig. 2

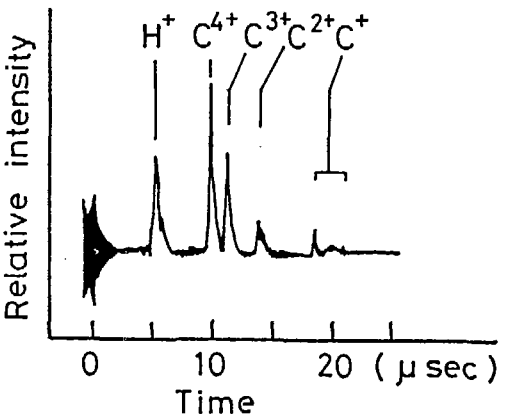

Fig. 3

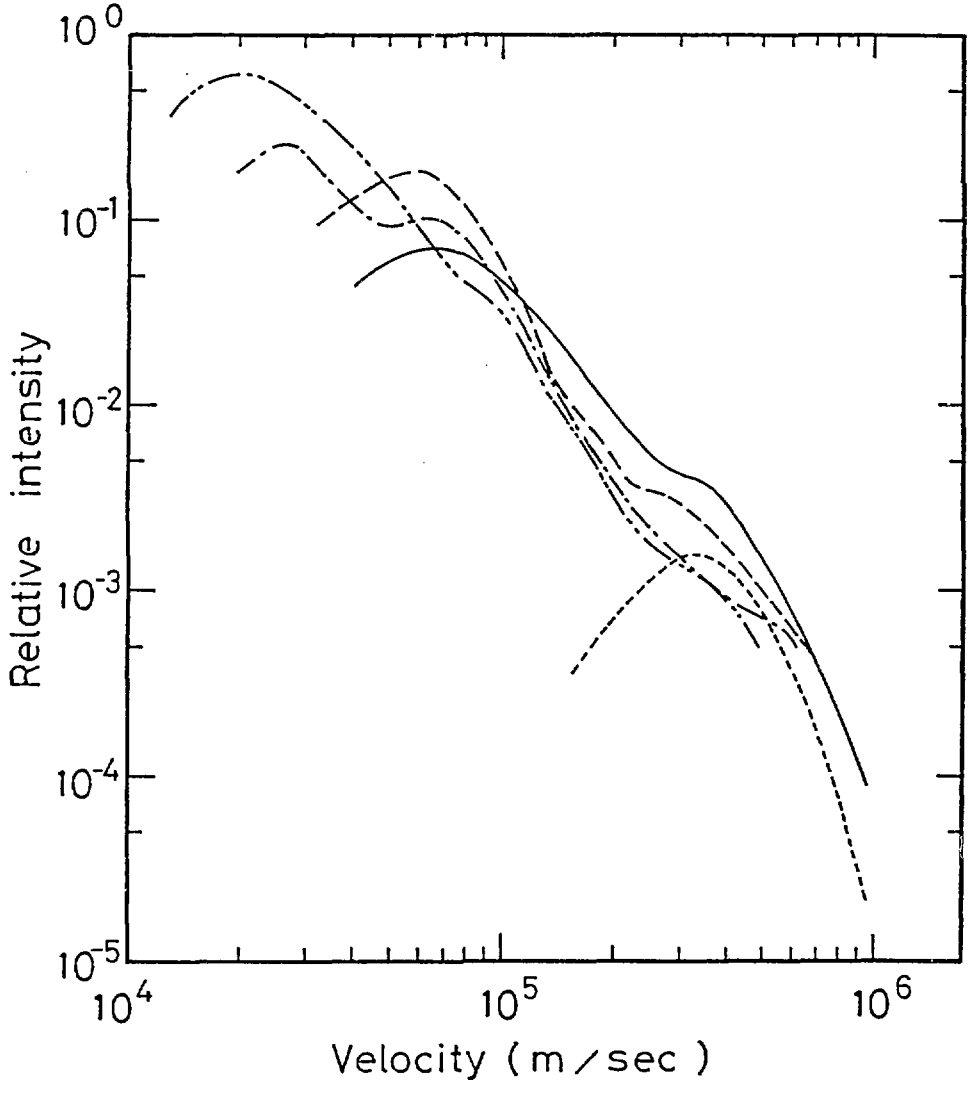
10^0
10^{-1}
10^{-2}
10^{-3}
10^{-4}
10^{-5}
Relative intensity
10^4
10^5
10^6
Velocity (m / sec)

Fig. 4

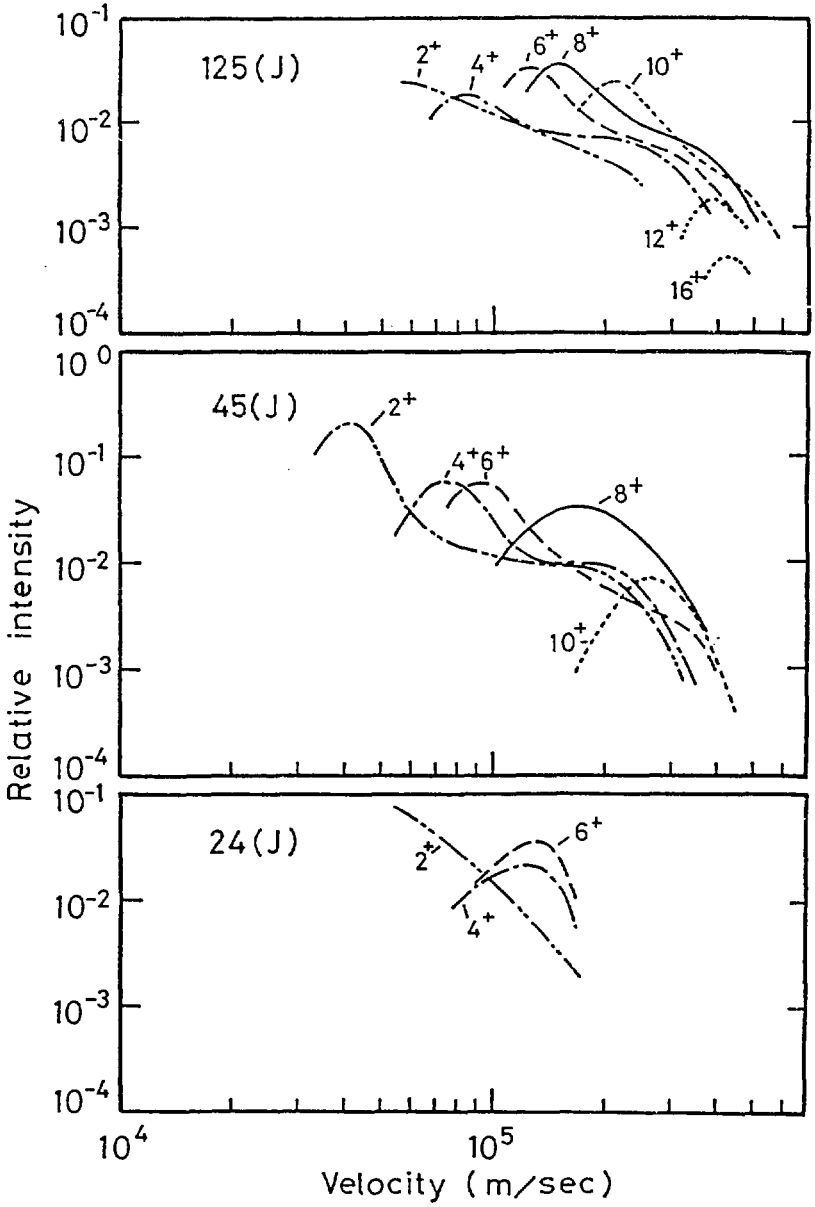
125(J)
45(J)
24(J)
2+
4+
6+
8+
10+
12+
16+
Relative intensity
Velocity (m/sec)
10^-1
10^-2
10^-3
10^-4
10^0
10^4
10^5

Fig. 5

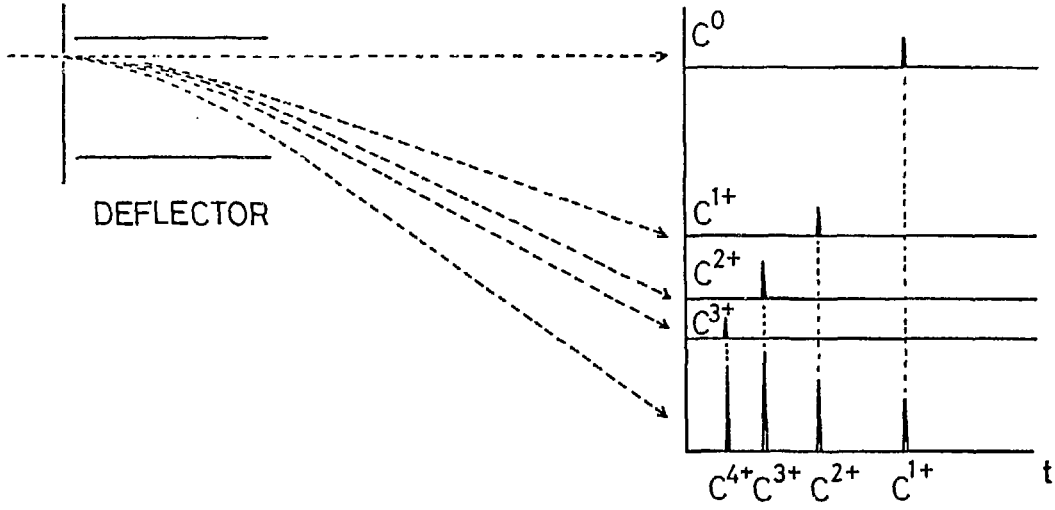

Fig.6

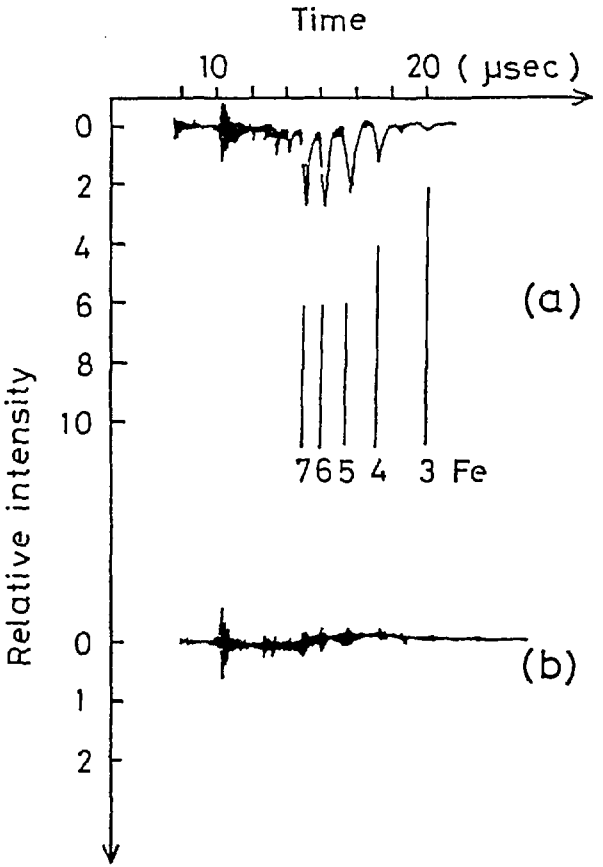

Fig.7

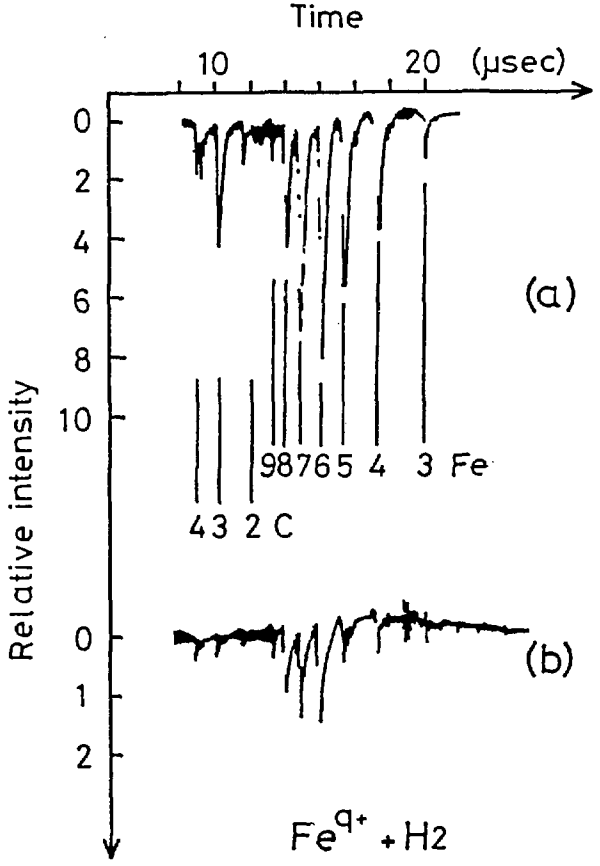
Time
10
20
(μsec)
0
2
4
6
8
10
Relative intensity
(a)
9 8 7 6 5 4 3 Fe
4 3 2 C
0
1
2
(b)
Fe^{q+} + H2

Fig. 8

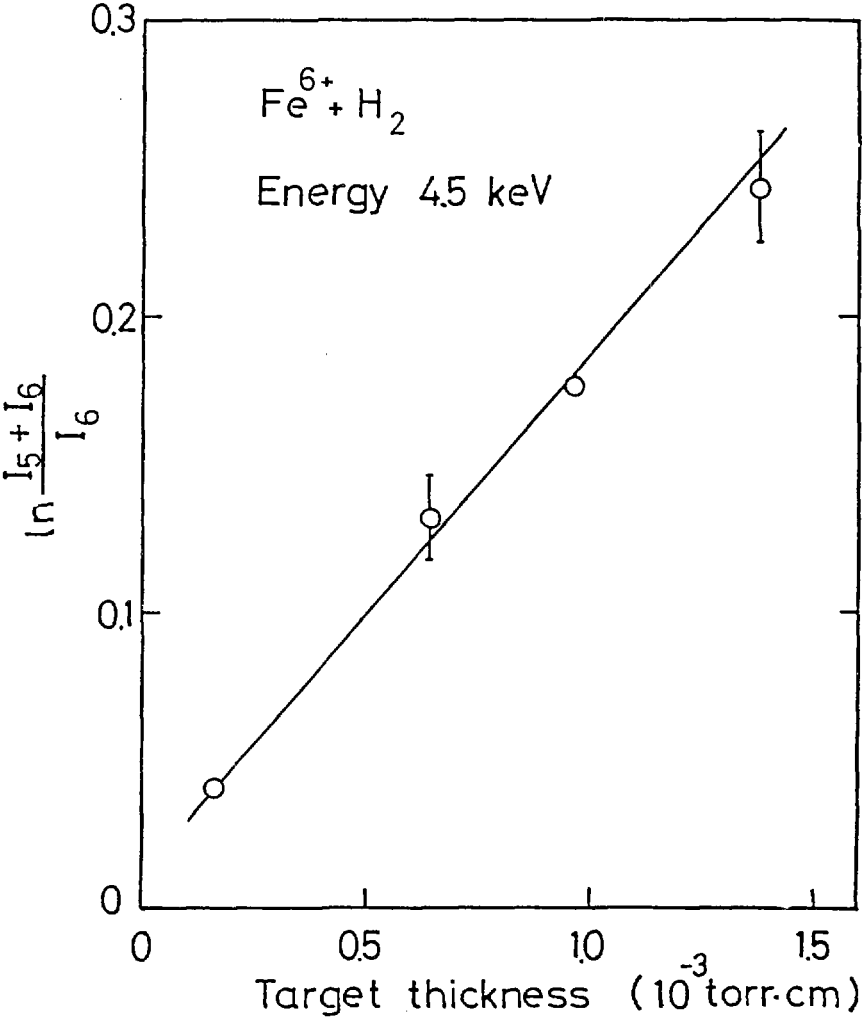
0.3
0.2
0.1
0
$Fe^{6+} + H_2$
Energy 4.5 keV
$\ln \frac{I_5 + I_6}{I_6}$
0
0.5
1.0
1.5
Target thickness (10^{-3} torr·cm)

Fig. 9

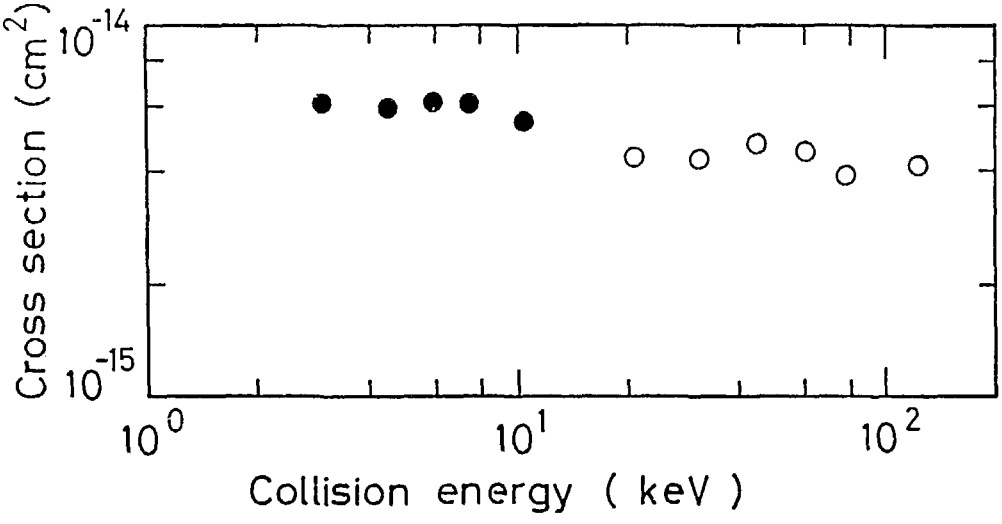
Cross section (cm^2)
10^{-14}
10^{-15}
10^0
10^1
10^2
Collision energy (keV)

Fig. 10